8

Potassium current deficit underlies thalamic hyperexcitability and seizures in Scn1a-deficient Dravet syndrome

Submitted to Nature Neuroscience:

S. Ritter-Makinson, A. Clemente-Perez, B. Higashikubo, E. Bennett, A. Chkaidze, O.H.J. Eelkman Rooda, M.-C. Cornet, F.E. Hoebeek, K. Yamakawa, M. Roberta Cilio, B. Delord, J.T. Paz

Dravet syndrome (DS) is a severe form of early-onset epileptic encephalopathy associated with intractable seizures, developmental delay, autistic features, sleep disorders, and sudden unexpected death. Approximately 80% of patients with DS have a loss-of-function mutation in one allele of the sodium channel gene SCN1A, which is mainly expressed in inhibitory neurons. The brain circuits causing seizures in these patients have not yet been identified, but runaway excitation has been thought to result from reduced activity in inhibitory neurons. Here, we show that runaway excitation results instead from enhanced activity in the inhibitory reticular thalamus, a region that regulates thalamocortical rhythms and contains intrinsically oscillatory neurons. In a well-established mouse model of a human Scn1a mutation, we found that reticular thalamic cells exhibited abnormally high pacemaker burst firing due to reduced SK current, which is conducted by a subfamily of calcium-activated potassium channels that normally limit firing. The dorsal thalamic complex was hyperexcitable in Scn1a mutant mice, as indicated by abnormally long evoked circuit oscillations. In vivo, we observed that non-convulsive seizures also occur in Scn1a mutant mice, and have similar EEG signatures as in humans with DS. These cellular abnormalities and seizures were all rescued by enhancing SK currents in the reticular thalamus. Further, optogenetically toggling between burst and tonic firing

in thalamic neurons launched and aborted seizures, respectively. Finally, computational modeling and electrophysiology indicate that reticular thalamic hyperexcitability can cause abnormal bursting in thalamocortical relay neurons to promote cortical seizure expression. These correlational, loss-of-function, and gain-of-function results support a model in which the most common and intractable seizures in DS are caused by a hypoactive SK current that makes the reticular thalamus hyperexcitable. Our study identifies the SK current as a novel therapeutic target in Dravet syndrome.

8.1 Introduction

The SCN1A gene encodes the alpha subunit of the voltage-gated sodium channel Nav1.1, which is widely expressed in the brain and the heart. As a key regulator of cardiac and brain rhythms, mutations in SCN1A dramatically affect human health. SCN1A is one of the most commonly mutated genes associated with epilepsy, including Dravet syndrome (DS) [449, 450]. This age-dependent, early-onset epileptic encephalopathy is characterized by intractable seizures, developmental delay, intellectual and motor disabilities, autistic features, sleep impairment, and high risk of sudden unexplained death. Reduced Scn1a function in GABAergic cortical and hippocampal inhibitory neurons is thought to reduce action potential (AP) firing and network inhibition, leading to runaway excitation (altered excitatory/inhibitory balance) and deadly seizures [451-454]. Global knockout of Scn1a in parvalbumin and somatostatin neurons increases susceptibility to thermally induced seizures, whereas selective knockout in either neuron subtype phenocopies distinct DS neuropsychiatric behavioral phenotypes [455]. However, the molecular and brain circuit mechanisms by which reduced SCN1A causes seizures is unknown. Uncovering how SCN1A mutations disrupt brain function could identify novel therapeutic strategies. SCN1A is abundant in the GABAergic nucleus reticularis thalami (nRT) [456], a brain structure known as the "guardian of the gateway" because of its role in dynamically modulating interactions between the thalamus and cerebral cortex [442, 457]. Scn1a–expressing GABAergic neurons of the nRT are intrinsic oscillators that inhibit the excitatory relay thalamus [458, 459], positioning them to regulate thalamocortical oscillations, including seizures. Given the abundant expression of Scn1a in nRT and the disruptions in nRT that correlate with neurological [460, 461] and psychiatric disorders [462, 463], we tested the hypothesis that Scn1a deficiency in nRT neurons is causally involved in DS in a well-established mouse model containing a human Scn1a mutation [452]. Mice with Scn1a haploinsufficiency due to this mutation are hereafter referred to as Scn1a DS mice.

8.2 Results

8.2.1 Scn1a deficiency leads to thalamic microcircuit hyperexcitability

Interactions between nRT and thalamocortical relay neurons generate rhythmic circuit oscillations. Because nRT neurons express high levels of Scn1a, [456] we asked whether the intra-thalamic micro-circuit rhythmogenesis is altered in Scn1a DS mice. We used horizontal thalamic slice preparations that conserve the connectivity between the nRT and 86 the ventrobasal complex of the somatosensory thalamus (VB) to assess nRT-VB

intrathalamic network oscillations independent of other structures (i.e., cortex) (**Fig. 1a, c**) [464].

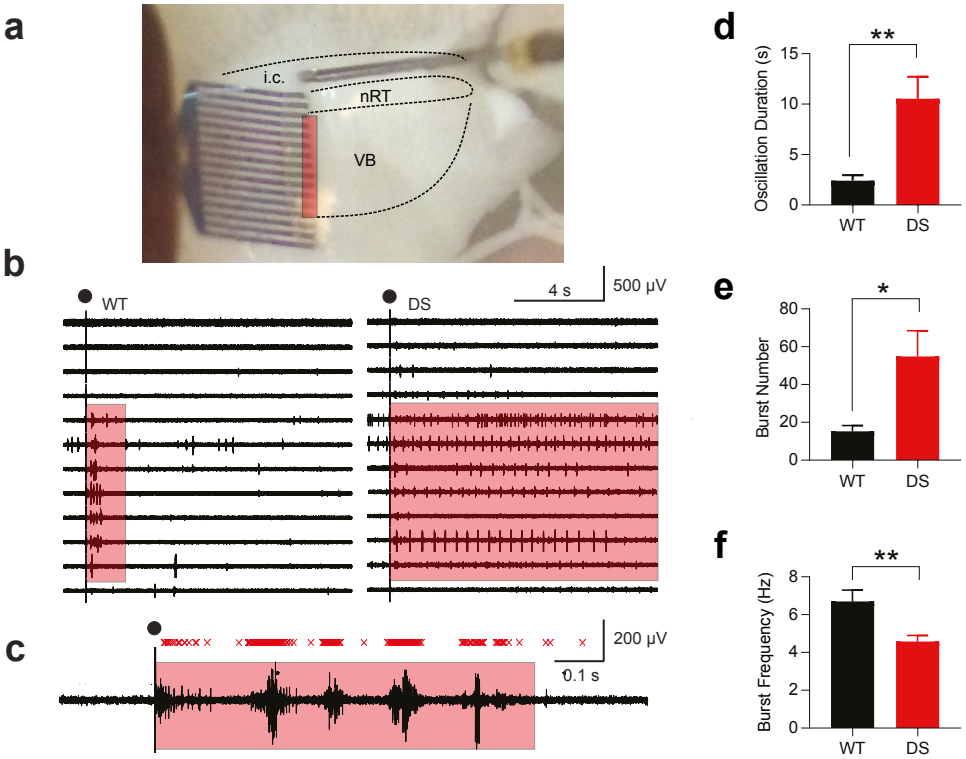

Figure 1. Scn1a deficiency in nRT neurons enhances intra-thalamic circuit oscillations.

a, Horizontal slice preparation to study intra-thalamic circuit oscillations. Position of 16-channel linear array silicon probe showing the region of the ventrobasal thalamus studied. Evoked oscillations were elicited via stimulation of the internal capsule. b, Representative example of evoked intra-thalamic circuit oscillations in slices prepared from WT and Scn1a DS mice. Black circles indicate stimulation artifact. Pink box indicates region of analysis in which evoked oscillations were observed. c, Detection of extracellular multiunit spikes (red "X") and bursts that compose a thalamic oscillation (duration is marked by orange box). Oscillation example taken from a slice prepared from a WT mouse. d, Duration of evoked oscillation. Mann-Whitney U test. WT: n = 9 mice, Scn1a DS: n = 12 mice. ** $p < 0.01$. e, Number of bursts within the evoked oscillation. Mann-Whitney U test. WT: n = 9 mice, Scn1a DS: n = 12 mice. * $p < 0.05$. f, Interburst interval within the evoked oscillation. Mann-Whitney U test. WT, n = 9 mice, DS, n = 12 mice. ** $p < 0.01$. Abbreviations: i.c., internal capsule; nRT, thalamic reticular nucleus; VB, ventrobasal somatosensory complex of the thalamus; WT, wild-type; DS, Scn1a Dravet syndrome.

Stimulation of the internal capsule consistently evoked rhythmic oscillatory bursting activity in VB (**Fig. 1b, left, C**), in the spindle frequency range (~10 Hz), similar to reports using electrical stimulation to activate intra-thalamic oscillations [126, 325, 464] or optogenetic activation in vivo [465]. Similar stimulations in Scn1a DS mice induced more bursts and

longer circuit oscillations in the thalamus (**Fig. 1b, right,** and **d, e**), with slower circuit oscillations in Scn1a DS mice (**Fig. 1f**). Thus, the nRT-VB microcircuit is hyperexcitable in Scn1a DS mice. This finding is surprising, given that nRT-VB 5 oscillations require robust firing in nRT neurons, which we expected to be lower in Scn1a-deficient mice, as reported [466].

8.2.2 Scn1a deficiency leads to enhanced high-frequency burst firing in nRT neurons

The nRT-VB microcircuit loop regulates rhythm generation, because thalamocortical VB cells fire low-threshold-spike (LTS)-mediated rebound bursts after hyperpolarization induced by nRT GABAergic inputs [467]. LTS-mediated burst firing is needed for the nRT to generate spindle oscillatory activity in the normal thalamocortical circuit [424, 468-470] and is also important for sensory processing [471, 472]

To determine if nRT-VB thalamic circuit hyperexcitability in Scn1a DS mice is explained by alterations in the electric membrane properties of nRT neurons, we performed whole-cell patch-clamp recordings of nRT neurons. We measured membrane potential changes in response to intracellular square current pulses (**Fig. 2a**). We studied PV-like bursting nRT cells because of their major involvement in thalamocortical rhythmogenesis. After similar responses to membrane potential hyperpolarizations, the number of APs within the initial rebound burst was ~1.5x higher in nRT neurons from Scn1a DS mice than 110 wild-type (WT) littermates (**Fig. 2a, b**). These data show that Scn1a mutation paradoxically enhances the post-inhibitory rebound bursts. We asked whether the prolonged rebound burst firing could result from enhanced T-type calcium currents that underlie the postinhibitory LTS and high-frequency burst firing [467]. We recorded T-currents from Scn1a DS and WT mice using identical steady-state inactivation (SSI) protocols (**Extended Data Fig. 1a**). The peak T-current density, voltage-dependence, and biophysical properties of the SSI T-type calcium currents were not altered in Scn1a DS nRT neurons (**Extended Data Fig. 1b-e**). These results show that enhanced post-hyperpolarization firing in Scn1a DS nRT neurons is not due to a stronger T-current. Since Scn1a was reduced in our DS mice, the AP threshold was depolarized, the AP width was increased as expected, and the input resistance was enhanced (**Extended Data Fig. 1**). The properties of spontaneous synaptic excitatory currents (sEPSCs) were not altered in nRT (**Extended Data Fig. 1**).

8.2.3 SK current deficit in nRT neurons underlies the enhanced cellular and circuit rhythmogenesis

Because burst firing in nRT neurons depends on interactions between T-type Ca2+ and small conductance calcium-activated (SK) K+ channels [473], we asked whether the function of SK channels was impaired in the Scn1a DS mice. Patch-clamp recordings showed that the density of SK currents in nRT neurons was reduced (**Fig. 2c, d**). Quantitative PCR for a predominant SK2 subtype in nRT [474] showed that mRNA levels of a variant of the SK2 channel (Kcnn2S) were reduced in nRT tissue isolated from DS mice (**Fig. 2d**). Notably, in a rescue experiment, we found that the SK agonist 1-ethyl-2-benzimidazolinone (EBIO) normalizes nRT bursting properties in Scn1a DS nRT neurons to WT levels (**Fig. 2e**).

In a biophysical model of an nRT neuron (**Fig. 2f**), reducing SK conductance was sufficient to account for the enhanced number of APs within the burst, as found in Scn1a DS nRT neurons (**Fig. 2g**). This increase proved general: the mean AP number in the entire DS parameter domain was larger than for WT (**Fig. 2h**, see Methods for domain definitions).

We assessed the impact of reduced SK conductance in the nRT neuron at the circuit level in a model, including thalamocortical (TC) and nRT neurons (**Fig. 3a**). We found that reduced SK phenocopied enhanced network oscillations (**Fig. 3b**), displayed longer oscillations (**Fig. 3c, d**), had more bursts within each oscillation (**Fig. 3e, f**), and showed lower oscillation frequency (**Fig. 3g, h**) in the DS domain, quantitatively predicting the features found in Scn1a DS thalamic circuits.

Mechanistically, in the DS condition, the increased number of APs per burst in the nRT neuron produces stronger inhibition and a larger post-inhibitory rebound in the TC neuron, which increased the excitatory TC-to-nRT feedback. Synaptic transmission was stronger in the circuit and more robust to noise, enabling more bursts and longer oscillations. The model showed how longer nRT bursts and TC inhibitory post-synaptic potentials explain the counterintuitive decrease in bursting frequency in DS mice. Remarkably, modifying the fast sodium conductance was not required to account for experimental results. Thus, reduced SK function in nRT neurons makes the thalamus "epileptic" by enhancing thalamic rhythmogenesis.

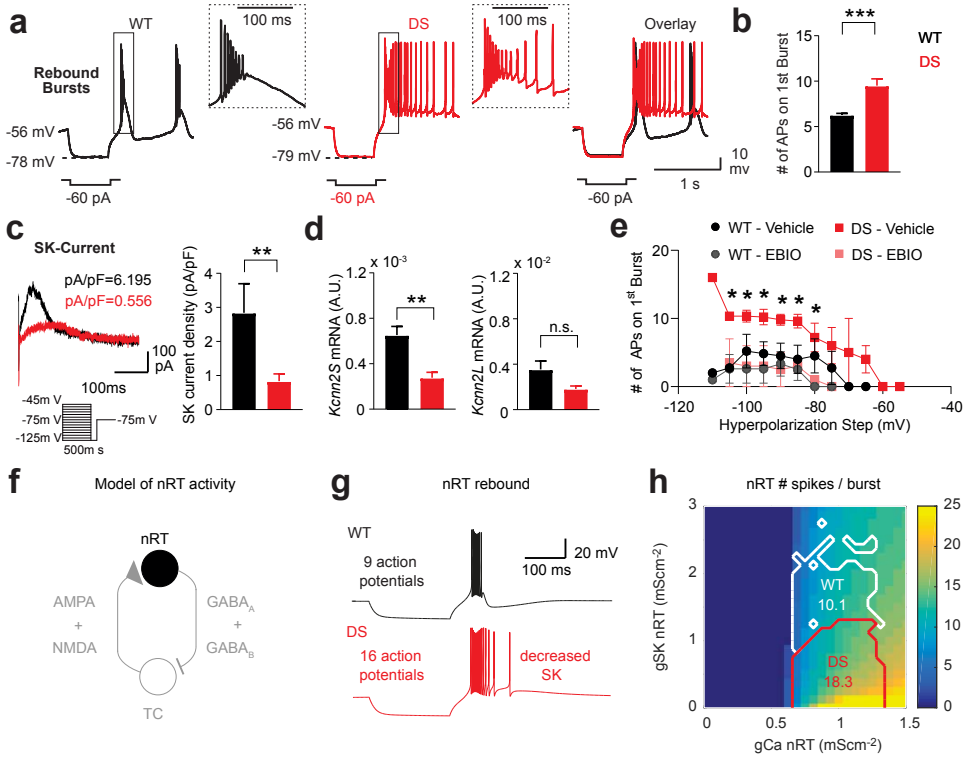

Figure 2. SK current deficiency in nRT neurons underlies the enhanced cellular bursting in Scn1a DS mice.

a, Representative traces showing that Scn1a DS neurons (red trace) exhibit enhanced post-inhibitory rebound burst firing upon hyperpolarization induced by −60 pA current pulses, compared to WT neurons (black trace). Insets show zoom of APs on first rebound burst. b, Number of APs on first rebound burst (WT: n = 30 cells, 4 mice; Scn1a DS, n = 43 cells, 6 mice). Data = mean ± SEM, compared with 14 parametric t-test with Welch's correction and α = 0.05, *** $p < 0.001$. c, Representative SK current traces obtained by digital subtraction in nRT neurons from WT (black) and Scn1a DS mutant (red) mice with respective current density. d. Left, Quantification of SK current density defined as the maximal current divided by individual cell capacitance. Data are represented as mean ± SEM, compared with Mann-Whitney U test (** $p = 0.0085$). WT: n = 8 cells, 3 mice; Scn1a DS: n = 10 cells, 3 mice. Right, SK2 relative mRNA expression levels (encoded by the gene Kcnn2, short and long transcript variants) normalized to Gapdh mRNA, in nRT. Expression levels were calculated using the ΔΔCT method and are expressed as arbitrary units. Mann-Whitney U test, ** $p < 0.01$. e, Number of APs on the first rebound burst, plotted against hyperpolarization step (mV) with vehicle or 100μM EBIO treatment. WT: n = 6 neurons, 3 mice; Scn1a DS: n = 6 neurons, 3 mice. Data = mean ± SEM. Data points compared by individual unpaired t-test, not corrected for multiple comparisons, * $p < 0.03$. f, Schematic of the minimal thalamic circuit used for computational modeling, including a thalamocortical (TC) and an nRT neuron, TC to nRT AMPA and NMDA excitatory synapses, and nRT to TC GABA–A and GABA–B inhibitory synapses. Synaptic currents are absent in the simulations of the nRT neuron mimicking intracellular recordings (**Figure 2g-h**). g, Voltage traces of a nRT neuron in the WT parameter domain (black trace; $\overline{g}_{CaT}^{nRT} = 0.85 mScm^{-2}$ and $\overline{g}_{SK}^{nRT} = 2 mScm^{-2}$) and of a neuron in the DS domain with decreased SK maximum conductance (red trace; $\overline{g}_{CaT}^{nRT} = 0.85 mScm^{-2}$ and $\overline{g}_{SK}^{nRT} = 0.1 mScm^{-2}$, in response to a hyperpolarizing injected current $I_{Inj}^{nRT} = -0.5 \mu A cm^{-2}$ for 500 ms h, Map of the average number of APs in the rebound burst in the nRT neuron model as a function of maximal conductance parameters. APs numbers are computed over 30 simulations with different realizations of the stochastic current mimicking the noise in the thalamic circuit. The mean of these average numbers of APs are indicated in the WT (white) and DS (red) domains. See Methods for the definition of WT and DS domains. Abbreviations: SK channel, small conductance calcium-activated potassium channels; WT, wild-type; DS, Scn1a Dravet syndrome; APs, action potentials; nRT, thalamic reticular nucleus; TC, thalamocortical.

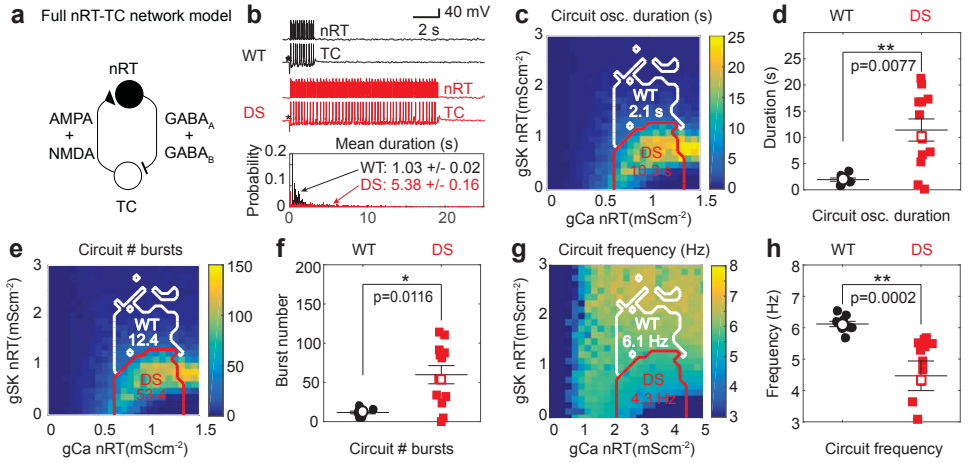

Figure 3. SK current deficiency in nRT underlies enhanced micro-circuit rhythmogenesis in SCN1A DS mice.

a, Schematic of the full nRT-TC circuit used for the computational modeling of thalamic oscillations in WT and DS conditions. b, (above) Example of nRT and TC voltage traces triggered by a stimulus (star) mimicking optogenetic stimulation, in the WT and DS conditions. (below) Probability distributions of the duration of oscillations in the circuit over 10^3 simulations with different realizations of the stochastic current. The mean oscillation duration in the TC-nRT circuit model in the DS condition was ~5 times that in the WT condition. The maximal conductances are as in **Figure 2g. c**, Map of the average oscillation duration of the TC-nRT circuit model as a function of maximal conductances, computed over 10^3 simulations with different realizations of the stochastic current. The mean of these averages in the WT and DS domains (white and red boundaries, respectively) are indicated. d, Duration of evoked oscillation for 9 samples with randomly maximal conductances drawn from the WT domain and 12 samples with randomly maximal conductances drawn from the DS domain. The difference of sample means is statistically significant (Mann–Whitney U test, WT: n = 9 mice, Scn1a DS: n = 12 mice. ** p = 0.0062). e, Same as in (c) for the average number of bursts of the oscillation. f, Same as in (d) for the average number of bursts of the oscillation. The difference of sample means is statistically significant (Mann– Whitney U test, WT: n = 9 mice, Scn1a DS: n = 12 mice. * p = 0.0208). g, Same as in (c) for the average frequency of the oscillation. h, Same as in (d) for the average frequency of the oscillation. The difference of sample means is statistically significant (Mann– Whitney U test, WT: n = 9 mice, Scn1a DS: n = 12 mice. ** p = 0.0002) Abbreviations: SK channel, small conductance calcium-activated potassium channels; WT, wild-type; DS, Scn1a Dravet syndrome; nRT, thalamic reticular nucleus; TC, thalamocortical.

8.2.4 "Silent" non-convulsive seizures are a major phenotype in human and mouse DS

Dravet syndrome presents with a complex seizure phenotype including multiple convulsive seizures – such as generalized tonic-clonic seizures (GTCS), myoclonic seizures, and febrile seizures – in addition to non-convulsive seizures – such as typical and atypical absence seizures. Notably, non-convulsive seizures are often intractable, contribute to the intellectual impairment observed in DS patients, and can progress in so-called obtundation status, resulting in a prolonged impairment of consciousness; yet, they are under-recognized and understudied, compared with convulsive seizures, mainly because they are clinically

difficult to diagnose. To date, non-convulsive seizures have not been described in the Scn1a DS mouse model. Thus, we set out characterize this phenotype in both human patients and our Scn1a DS mice (**Fig. 4 a-d**). Non-convulsive seizures occurred on average 15 ± 8 times per hour in mice, lasting 0.5-6 seconds (n=9 mice), and 7 ± 4 times 166 per hour in our human DS patient, lasting 10 seconds (n=1 patient). Notably, non- convulsive seizures in Scn1a DS mice and DS patients exhibited similar spectral EEG signatures with fundamental frequencies of 5-7 Hz (**Fig. 4**). To our knowledge, this study is the first to compare DS seizures in the Scn1a mouse model and human patients.

8.2.5 Optogenetic toggling of thalamic bursting bi-directionally modulates seizures in 172 SCN1A-deficient mice

We next asked whether the high-frequency burst firing in vitro in the thalamus occurs during spontaneous seizures in freely behaving mice. Optrode recordings in nRT (**Extended Data, Fig. 2d**) and VB (**Fig. 4g-i**) TC neurons showed high-frequency burst firing, phase-locked with spontaneously occurring non-convulsive seizures.

Notably, nRT does not project directly onto the cortex and thus exerts its effects on cortical rhythms through its TC targets. To test the causality of the nRT-VB pathway in non-convulsive seizures, which predominate in the S1 ECoG, we perturbed the VB firing using Stable Step Function Opsin (SSFO). SSFO is a bistable opsin, which was used to show that activation in TC cells causes depolarization and a switch from bursting to tonic firing [225]. We unilaterally activated SSFO in VB after seizure detection. SSFO activation reliably and rapidly eliminated TC bursts, toggled tonic firing, and stopped ongoing seizures (**Fig. 4g-j**). Thus, TC VB bursting output may be causally required to maintain non-convulsive seizures in DS. We tested more clinically tractable strategies for interrupting hyperthermia-triggered GTCS in DS patients using electrical stimulation. The spectrogram of these seizures showed a pronounced increase in broad gamma-band (30-100 Hz) power (**Extended Data, Fig. 3a, b**). Because we pinpointed the thalamus as a potential choke point for DS seizure control, we employed unilateral electrical stimulation of VB (**Extended Data, Fig. 3c, d**) and the anterior thalamic nuclei, (**Extended Data, Fig. 3e, f**) upon the start of temperature-induced GTCS in our Scn1a DS model. Moreover, we also investigated another potential clinical target – the medial and interposed cerebellar nuclei – which send divergent projections throughout the thalamic complex and modulate various cerebral cortical regions. Although no significant anti-epileptic effects were observed when unilaterally manipulating VB or AN, we did see a seizure-modifying effect of electrical stimulation of the cerebellar nuclei (**Extended Data, Fig. 3g, h**). Together, these data indicate that simultaneous recruitment of multiple thalamic nuclei and/or recruitment of thalamic nuclei together with parts of the cortex are more effective for modification of ongoing GTCS in DS.

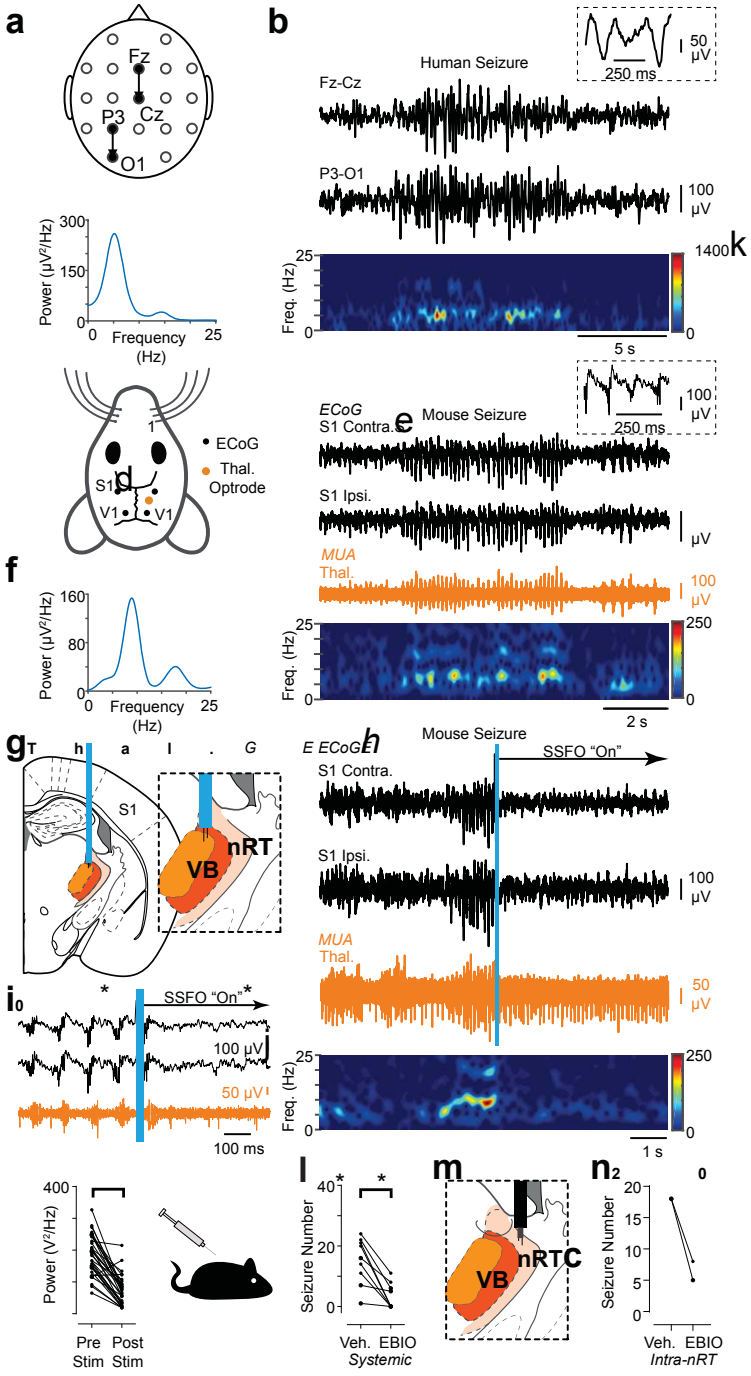

Figure 4. Dual strategy for seizure control in Dravet patients converge on the thalamus.

a, Diagram of human EEG recording montage. b, top: Example of the EEG signature of a typical non-convulsive seizure in a patient with DS recorded in two different locations on the scalp. inset, Note the spikes are not typical spike-and-wave discharges and have a higher frequency component in addition to the slower oscillation. bottom: Spectrogram showing frequency components of the recorded seizure. c, Power spectral density of the seizure shown in b. Note the peak fundamental frequency is ~5 Hz. d, Diagram of the mouse ECoG and thalamic depth electrode recording montage. ECoG was recorded from somatosensory (S1) and visual (V1) cortices, with depth electrodes implanted in the thalamus. e, top: Example of an ECoG signature of a typical non-convulsive seizure in Scn1a DS mice recorded from S1 (black), along with simultaneous multi-unit (MU) recordings in the thalamus (orange). inset, Note the spikes are not typical spike-and-wave discharges and have a higher frequency component in addition to the slower oscillation. bottom: Spectrogram showing frequency components of the recorded seizure. f, Power spectral density of the seizure shown in e. Note the peak fundamental frequency is 6–7 Hz. g, Diagram of optogenetic targeting of the thalamus. inset, Depth electrodes were positioned in VB thalamus. h, top: Example of optogenetic seizure interruption of an ongoing non-convulsive seizure in a Scn1a DS mouse. The blue bar corresponds to a brief (50 ms) pulse of blue light to activate SSFO-expressing thalamocortical neurons. Unilateral activation of SSFO in the thalamus immediately interrupts an ongoing seizure. bottom: Spectrogram showing frequency components of the recorded seizure and decrease in power after SSFO activation. i, Magnification of the seizure interruption shown in (h). Activation of SSFO switches rebound burst firing in the thalamus to tonic firing. j, Quantification of 1-25 Hz broadband power 2 s before and after optogenetic manipulation. Data are from 32 trials across 4 mice. **** $p < 0.0001$ Mann-Whitney test. k, Diagram of systemic administration of EBIO (s.c. 25 mg/kg). l, Quantification of effects of systemic administration of EBIO (25 mg/kg, s.c.) on non-convulsive seizure number within 30 minutes of EBIO infusion. Data are from n = 9 Scn1a DS mice. ** $p = 0.0039$ Wilcoxon Signed-Rank test. m, Diagram of unilateral intra-nRT infusion of EBIO in conjunction with simultaneous multiunit recordings. n, Quantification of effects of intra-nRT administration of EBIO (800 nl of 0.4 mM) on non-convulsive seizure number within 1 hour of infusion. Data are from n = 2 Scn1a DS mice. Abbreviations: EEG, electroencephalogram; S1, somatosensory cortex; V1, visual cortex; ECoG, electrocorticogram; Thal., thalamus; Ipsi., ipsilateral; Contra., contralateral; MUA, multiunit activity; VB, ventrobasal thalamus; nRT, thalamic reticular nucleus; SSFO, stable step-function opsin.

We next asked whether mimicking rhythmic hyperpolarization in the nRT-to-VB pathway was sufficient to cause seizures during normal baseline behavior. We expressed halorhodopsin (eNpHR) in TC neurons as in Sorokin et al. (2017) and showed that unilaterally driving TC bursting causes bilateral GTCS in Scn1a DS mice (**Extended Data, Fig. 4**). The finding is striking, given that TC neurons of primary thalamic nuclei project exclusively to ipsilateral cortex. These results suggest the nRT-VB pathway is sufficient to initiate and necessary to maintain seizures in Scn1a DS mice.

8.2.6 SK enhancement treats seizures in SCN1A-deficient mice

Next we asked whether pharmacological boosting of SK channels could rescue seizures in Scn1a DS mice. Acute injection of EBIO, either systemically or locally in the nRT, reduced the number of spontaneously occurring non-convulsive seizures in Scn1a DS mice (**Fig. 4k-n**). These results support the idea that a reduction in SK channels in nRT underlies behavioral epileptic seizures in DS.

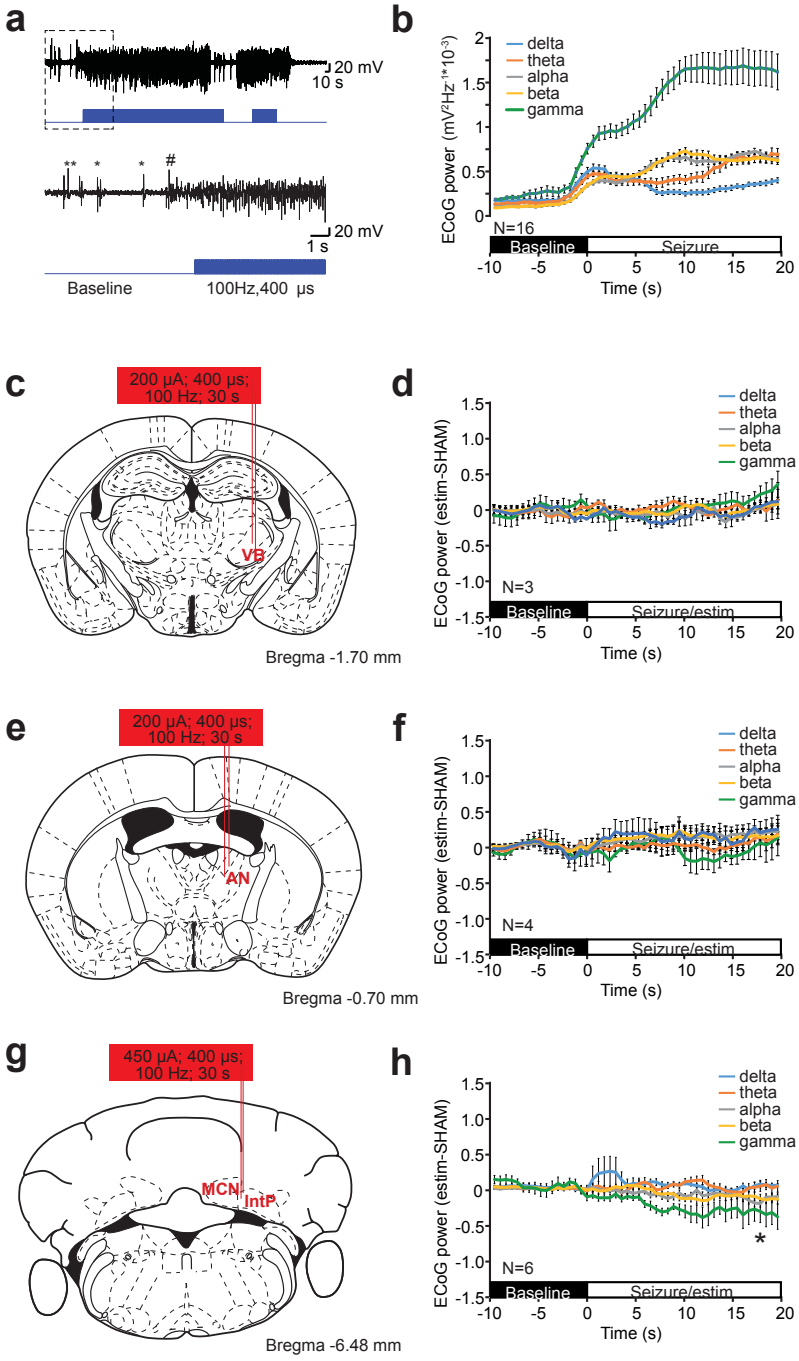

Extended Data Figure 3. Hyperthermia-triggered GTCS cannot be halted by thalamic or cerebellar stimulation.

a) ECoG recorded from S1 electrodes in a freely moving mouse indicates the clear onset of seizure-related activity. Manually started electrical stimulation (in this case sham condition is shown) was triggered after GTCS onset (pound sign). Asterisks indicate myoclonic jerks that precede seizure onset. b) Using a line length algorithm we determined the onset of the seizures and aligned the recordings of GTCS seizures from 16 mice. Note the steep increase in ECoG power at the gamma band (30-100 Hz) upon seizure onset. c) Schematic representation of stimulus electrode location in the ventral basal nucleus of the thalamus (VB). d) Difference in ECoG power at various frequency band between electrical stimulation (estim) and sham stimulation experiments. No consistent effect was observed (Wilcoxon-Signed Rank Test, n = 3 mice, all bands n.s.). e-h) Similar to (c,d) but for AN and CN stimulation experiments, respectively. Note, * in (h) corresponds to p = 0.046 for significant reduction in gamma power between 5 s of seizure (sham) versus 5 s of stimulation (estim) using a Wilcoxon-Signed Rank Test (AN, n = 4 DS mice, all bands n.s.; CN n = 6 DS mice, all bands except gamma n.s.).

Stereotactic atlas panels were adapted from Paxinos atlas for mouse brain (3rd edition). Error bars indicate SEM. Abbreviations: ECoG, electrocorticogram; S1, somatosensory cortex; GTCS, generalized tonic-clonic seizure; VB, ventral basal thalamus; AN, anterior nuclei of the thalamus; CN; cerebellar nuclei; MCN; medial cerebellar nucleus; IntP, interposed cerebellar nucleus.

8.3 Discussion

Using a well-established model of DS with Scn1a haploinsufficiency, we uncovered a novel and unexpected mechanism to explain intractable seizure pathology in DS, whereby Scn1a reduction, together with reduced SK current in nRT, drives thalamic hyperexcitability to promote cortical seizures.

Unlike previous work showing that dissociated cells from the GABAergic nRT of Scn1a-deficient mice are hypoexcitable and fire fewer APs, we find in the intact thalamic circuit in a comparable Scn1a-deficient model of DS that nRT neurons are hyperexcitable: they are more likely to fire bursts of APs. We show that this paradoxical increase in cell firing results from a compensatory decrease in SK2 channel expression and membrane conductance in nRT neurons. Our findings are distinct from previous work on DS, which suggested that sodium channel deficits in inhibitory neurons result in reduced firing and reduced network inhibition in neocortex and hippocampus to promote seizures [386, 451, 452, 454]. Moreover, our results contrast with another study in which a missense mutation in Scn1a associated with genetic epilepsy with febrile seizures resulted in reduced firing in nRT neurons. Instead, our data suggest that thalamic circuit dysfunction and seizure pathology in DS involve complex interactions among Scn1a, its particular mutation, and the brain circuits in which Scn1a is found. Our results support the view that DS pathology cannot simply be explained by cortical inhibitory neuron hypoexcitability by defining a novel role for Scn1a in the thalamus.

Identification and manipulation of SK2 as a modifier of DS seizures is novel and expands upon the growing list of genetic modifiers of SCN1A-epilepsies. Notably, our study not only found that Kcnn2 is reduced in the thalamus, but that pharmacological enhancement of SK2

can treat seizures in our Scn1a DS mouse model. Additionally, our findings complement existing literature on SK2 function in thalamic circuitry and other symptoms associated with DS. Notably, mice lacking SK2 show fragmented sleep patterns and reduced sleep spindles similar to DS mice, supporting the idea that reductions in SK2 underlie thalamic circuit dysfunction and its associated sleep impairments in DS. Overexpressing SK2 increases sleep spindles and reduces sleep fragmentation, further supporting that enhancement of SK2 function in DS might restore sleep impairments, in addition to treating intractable seizures.

To our knowledge, we are also the first to describe and define a mechanism for non-convulsive seizures in DS and compare this phenomenon with human patients. Although understudied, non-convulsive seizures are often intractable and may account for the cognitive decline, behavioral disorders, and reduction in social life associated with DS. Interestingly, the absence of non-convulsive seizures is typical of borderline forms of DS, in which cognitive ability is at least partially preserved, as reported in 1987.

Indeed, non-convulsive seizures, in particular atypical absence seizures, are co-morbid with autism spectrum disorders in multiple mouse models. By identifying the SK current as a novel therapeutic target for the non-convulsive seizures in DS, we also posit that enhancing SK function might treat deficits in cognition and social interaction in DS.

Given the recently uncovered framework of nRT organization and function, we hypothesize that the nRT is a key brain substrate responsible for the co-morbidity between neurological (seizure) and psychiatric (autism) components in DS. Within this framework, we propose that the nRT, through its respective projections to sensory and limbic thalamocortical nuclei, underlies the complex intractable seizures and autism, respectively, in DS. This nucleus thus can act as a final common pathway to treat the multi-faceted DS.